Friction **11**(6): 1107–1120 (2023)
https://doi.org/10.1007/s40544-022-0656-z
ISSN 2223-7690
CN 10-1237/TH
RESEARCH ARTICLE

Subloading-friction model with saturation of tangential contact stress

Koichi HASHIGUCHI[1,2,*], **Masami UENO**[3]

[1] *Kyushu University, Fukuoka 819-0395, Japan*

[2] *MSC Software Ltd., Tokyo 101-0054, Japan*

[3] *University of the Ryukyus, Okinawa 903-0213, Japan*

Received: 28 January 2022 / Revised: 04 March 2022 / Accepted: 23 May 2022

Abstract: The incorporation of the saturation of the tangential contact stress with the increase of the normal contact stress is required for the analysis of the friction phenomenon of solids and structures subjected to a high normal contact stress, which cannot be described by the Coulomb friction condition, in which the tangential contact stress increases linearly with the increase of the normal contact stress. In this article, the subloading-friction model, which is capable of describing the smooth elastic–plastic transition, the static–kinetic transition, and the recovery of the static friction during the cease of sliding, is extended to describe this property. Further, some numerical examples are shown, and the validity of the present model will be verified by the simulation of the test data on the linear sliding of metals.

Keywords: high contact stress; monotonic/reciprocal sliding; static/kinetic friction; subloading-friction model

1 Introduction

All bodies in the natural world are exposed to the friction phenomena, contacting with the other bodies. Therefore, it is indispensable to analyze the friction phenomena rigorously in addition to the deformation behaviors of the contact bodies themselves.

Here, it should be noticed that the friction is the typical irreversible, i.e., plastic phenomenon, so that it should be formulated within the framework of the elastoplasticity theory. Then, the various friction models in the elastoplasticity have been formulated as the rigid-plasticity [1, 2] and the perfect-plasticity [3–10]. However, these past formulations fall within the conventional plasticity assuming that the interior of the sliding-yield surface is the purely-elastic domain, so that the accumulation of plastic sliding during the cyclic loading of the tangential contact stress as seen in the loosening of the bolt and nut cannot be predicted. In addition, the simple friction model [11] falling within the framework of the creep model without the sliding yield surface was formulated, but the creep model is inapplicable to the general sliding velocity, since the creep sliding is induced in any low stress level as delineated by Hashiguchi [12, 13], and thus it was applied only to the simulation of the sliding behavior at high sliding velocity [14]. Eventually, it is irrelevant to the usual sliding behavior including the quasi-static sliding.

Further, various friction models regardless to the elastoplasticity have been proposed hitherto so that they are limited to the one-dimensional sliding behavior represented by the rate-and-state model [15–21] and the fundamentally-irrational models [22–27] involving the time itself in order to describe the recovery of the friction coefficient caused by the cease of sliding have been proposed, which result in the loss of the objectivity as the constitutive relation [28, 29]. The loss of the objectivity is evident from the fact that the evaluation of elapsed time is accompanied with the

* Corresponding author: hashikoi87@gmail.com

Nomenclature

$\bar{\boldsymbol{u}}$, $\bar{\boldsymbol{u}}_{\mathrm{n}}$, $\bar{\boldsymbol{u}}_{\mathrm{t}}$	Sliding displacement vector and its normal part and tangential part	$\boldsymbol{n}_{\mathrm{t}}$	Unit direction vector of plastic sliding rate, which is the tangential component of outward-normal vector to sliding subloading surface
$\bar{\boldsymbol{u}}^{\mathrm{e}}$, $\bar{\boldsymbol{u}}_{\mathrm{n}}^{\mathrm{e}}$, $\bar{\boldsymbol{u}}_{\mathrm{t}}^{\mathrm{e}}$	Elastic sliding displacement vector and its normal part and tangential part	r	Sliding normal-yield ratio
$\bar{\boldsymbol{u}}^{\mathrm{p}}$, $\bar{\boldsymbol{u}}_{\mathrm{n}}^{\mathrm{p}}$, $\bar{\boldsymbol{u}}_{\mathrm{t}}^{\mathrm{p}}$	Plastic sliding displacement vector and its normal part and tangential part	$\bar{U}(r)$	Function in evolution of r
$\bar{u}_{\mathrm{t}}$	Tangential component of sliding displacement vector to contact surface	μ	Sliding hardening function
$\boldsymbol{t}_{\bar{\mathrm{u}}}$	Unit tangential sliding vector	μ_{s}, μ_{k}	Material constant specifying the maximum (static) and minimum (kinetic) values of μ,
$\boldsymbol{f}$, $\boldsymbol{f}_{\mathrm{n}}$, $\boldsymbol{f}_{\mathrm{t}}$	Contact stress vector and its normal part and tangential part	κ, ξ	Material constant designating the decrease of hardening function by plastic sliding and recovery of hardening function by time-elapse
f_{n}, f_{t}	Normal and tangential components of contact stress vector to contact surface	$\dot{\bar{\lambda}}$, $\dot{\bar{\Lambda}}$	Positive plastic multiplier in terms of stress rate and strain rate
$\boldsymbol{t}_{\mathrm{f}}$	Unit tangential contact stress vector	m^{p}, m^{c}	Sliding plastic modulus and creep modulus
w^{e}	Elastic sliding work	$\bar{\boldsymbol{E}}^{\mathrm{ep}}$	Elastoplastic sliding modulus tensor
$\varphi(\bar{\boldsymbol{u}}^{\mathrm{e}})$	Elastic sliding energy function	g_{n}	Function describing dependence of normal contact stress on contact stress ratio
$\bar{\boldsymbol{E}}$	Elastic sliding modulus tensor	c_{n}	Material constant dominating inclination of sliding-yield surface at null normal contact stress
α_{n}, α_{t}	Elastic sliding coefficient in normal and tangential directions		
$f(\boldsymbol{f})$	Sliding-yield function of sliding stress vector		
$\boldsymbol{n}$	Unit outward-normal vector to contact surface		

ambiguity in the judgment about when the sliding commences and ceases, especially in the state that the sliding velocity varies in a low-velocity region. Besides, the Coulomb friction equation with the nonhardening friction yield surface enclosing the purely-elastic domain is adopted widely in the commercial finite element method (FEM) software, e.g., Abaqus, Marc, etc., and explained extensively in the well-known monographs (e.g., Refs. [30, 31]). It is merely capable of describing the constant friction coefficient independent of the sliding displacement.

The subloading-friction model (Hashiguchi et al. [32, 33]) is capable of describing the smooth elastic–plastic transition, the reduction of friction coefficient from the static to the kinetic friction, the recovery to the static friction during the cease of sliding, etc. It has been applied to the metal friction [32, 33], the metal-to-soil friction [34] and the stick–slip behavior [35]. Further, it has been extended to describe the orthotropic anisotropy [36, 37] and the viscoplastic sliding behavior for the lubricated (wet) friction [38].

Now, it should be recognized that the tangential contact stress increases but saturates with the increase of normal contact stress. This property is of crucial importance for the predictions of the friction behaviors in the fastening of bolts and nuts, the wedge driving or penetration, the compression of solid body, the strip rolling processing of metal plates, the earthquake occurrence caused by the sliding phenomenon between continental plates and oceanic plates, etc., in which high normal contact stresses are applied. However, it cannot be described by the Coulomb friction condition [12, 13], in which the tangential contact stress increases linearly with the normal contact stress. Then, the formulations of the subloading-friction model taking account of this property have been proposed by Hashiguchi et al. [32, 33] and Ozaki et al. [39]. However, the former

formulations [32, 33] adopting the teardrop-type or the parabola-shaped sliding yield surface involve the physical irrationality that the tangential contact stress decreases with the increase of the normal contact stress in a high normal contact stress region, and the latter formulation [39] is irrelevant to solid materials as metals but limited to the rubbers.

In this article, the rigorous subloading-friction model incorporating the sliding-yield stress function, in which the tangential contact stress increases but saturates with the increase of the normal contact stress, will be formulated, and the numerical examples for the monotonic and the reciprocal sliding under several levels of normal contact stress with various stationary time of sliding will be shown, adopting the present model. Further, the validity of the present model will be verified by the simulation of the test data [14] on the linear sliding between metals.

2 Sliding displacement and contact stress

The sliding displacement vector $\overline{\boldsymbol{u}}$, which is defined as the relative sliding displacement of the counter (slave) body to the main (master) body, is orthogonally decomposed into the normal sliding displacement vector $\overline{\boldsymbol{u}}_{\mathrm{n}}$ and the tangential sliding displacement vector $\overline{\boldsymbol{u}}_{\mathrm{t}}$ to the contact surface as Eq. (1) [13, 40]:

$$\overline{\boldsymbol{u}} = \overline{\boldsymbol{u}}_{\mathrm{n}} + \overline{\boldsymbol{u}}_{\mathrm{t}} \tag{1}$$

where

$$\begin{cases} \overline{\boldsymbol{u}}_{\mathrm{n}} = (\overline{\boldsymbol{u}} \cdot \boldsymbol{n})\boldsymbol{n} = (\boldsymbol{n} \otimes \boldsymbol{n})\overline{\boldsymbol{u}} = -\overline{u}_{\mathrm{n}}\boldsymbol{n} \\ \overline{\boldsymbol{u}}_{\mathrm{t}} = \overline{\boldsymbol{u}} - \overline{\boldsymbol{u}}_{\mathrm{n}} = (\boldsymbol{I} - \boldsymbol{n} \otimes \boldsymbol{n})\overline{\boldsymbol{u}} \end{cases} \tag{2}$$

$$\begin{cases} \overline{u}_{\mathrm{n}} \equiv -\boldsymbol{n} \cdot \overline{\boldsymbol{u}}_{\mathrm{n}} = -\boldsymbol{n} \cdot \overline{\boldsymbol{u}} \\ \overline{u}_{\mathrm{t}} = \boldsymbol{t}_{\bar{\mathrm{u}}} \cdot \overline{\boldsymbol{u}} = \| \overline{\boldsymbol{u}}_{\mathrm{t}} \|, \boldsymbol{t}_{\bar{\mathrm{u}}} \equiv \dfrac{\overline{\boldsymbol{u}}_{\mathrm{t}}}{\| \overline{\boldsymbol{u}}_{\mathrm{t}} \|} (\boldsymbol{n} \cdot \boldsymbol{t}_{\bar{\mathrm{u}}} = 0, \ \| \boldsymbol{t}_{\bar{\mathrm{u}}} \| = 1) \end{cases} \tag{3}$$

$\boldsymbol{n}$ is the unit outward-normal vector of the surface of main body, and $\boldsymbol{I}$ denotes the second-order identity tensor. The minus sign is added for $\overline{u}_{\mathrm{n}}$ to be positive when the counter body approaches the main body.

The sliding displacement vector $\overline{\boldsymbol{u}}$ can be exactly decomposed into the elastic sliding displacement $\overline{\boldsymbol{u}}^{\mathrm{e}}$ and the plastic (irreversible) sliding displacement $\overline{\boldsymbol{u}}^{\mathrm{p}}$ in the additive form even for the finite sliding displacement, i.e.,

$$\overline{\boldsymbol{u}} = \overline{\boldsymbol{u}}^{\mathrm{e}} + \overline{\boldsymbol{u}}^{\mathrm{p}} \tag{4}$$

$$\begin{cases} \overline{\boldsymbol{u}}^{\mathrm{e}} = \overline{\boldsymbol{u}}^{\mathrm{e}}_{\mathrm{n}} + \overline{\boldsymbol{u}}^{\mathrm{e}}_{\mathrm{t}} \\ \overline{\boldsymbol{u}}^{\mathrm{p}} = \overline{\boldsymbol{u}}^{\mathrm{p}}_{\mathrm{n}} + \overline{\boldsymbol{u}}^{\mathrm{p}}_{\mathrm{t}} \end{cases} \tag{5}$$

where

$$\begin{aligned} \overline{\boldsymbol{u}}^{\mathrm{e}}_{\mathrm{n}} &= (\overline{\boldsymbol{u}}^{\mathrm{e}} \cdot \boldsymbol{n})\boldsymbol{n} = (\boldsymbol{n} \otimes \boldsymbol{n})\overline{\boldsymbol{u}}^{\mathrm{e}} \\ \overline{\boldsymbol{u}}^{\mathrm{e}}_{\mathrm{t}} &= \overline{\boldsymbol{u}}^{\mathrm{e}} - \overline{\boldsymbol{u}}^{\mathrm{e}}_{\mathrm{n}} = (\boldsymbol{I} - \boldsymbol{n} \otimes \boldsymbol{n})\overline{\boldsymbol{u}}^{\mathrm{e}} \end{aligned} \tag{6}$$

$$\begin{cases} \overline{\boldsymbol{u}}^{\mathrm{p}}_{\mathrm{n}} = (\overline{\boldsymbol{u}}^{\mathrm{p}} \cdot \boldsymbol{n})\boldsymbol{n} = (\boldsymbol{n} \otimes \boldsymbol{n})\overline{\boldsymbol{u}}^{\mathrm{p}} \\ \overline{\boldsymbol{u}}^{\mathrm{p}}_{\mathrm{t}} = \overline{\boldsymbol{u}}^{\mathrm{p}} - \overline{\boldsymbol{u}}^{\mathrm{p}}_{\mathrm{n}} = (\boldsymbol{I} - \boldsymbol{n} \otimes \boldsymbol{n})\overline{\boldsymbol{u}}^{\mathrm{p}} \end{cases} \tag{7}$$

The contact stress vector $\boldsymbol{f}$ acting on the main body is additively decomposed into the normal contact stress vector $\boldsymbol{f}_{\mathrm{n}}$ and the tangential contact stress vector $\boldsymbol{f}_{\mathrm{t}}$ as Eq. (8):

$$\boldsymbol{f} = \boldsymbol{f}_{\mathrm{n}} + \boldsymbol{f}_{\mathrm{t}} = -f_{\mathrm{n}}\boldsymbol{n} + f_{\mathrm{t}}\boldsymbol{t}_{\mathrm{f}} \tag{8}$$

where

$$\begin{cases} \boldsymbol{f}_{\mathrm{n}} = (\boldsymbol{n} \cdot \boldsymbol{f})\boldsymbol{n} = (\boldsymbol{n} \otimes \boldsymbol{n})\boldsymbol{f} = -f_{\mathrm{n}}\boldsymbol{n} \\ \boldsymbol{f}_{\mathrm{t}} = \boldsymbol{f} - \boldsymbol{f}_{\mathrm{n}} = (\boldsymbol{I} - \boldsymbol{n} \otimes \boldsymbol{n})\boldsymbol{f} = f_{\mathrm{t}}\boldsymbol{t}_{\mathrm{f}} \ \ (\boldsymbol{n} \cdot \boldsymbol{f}_{\mathrm{t}} = 0) \end{cases} \tag{9}$$

$$\begin{cases} f_{\mathrm{n}} = -\boldsymbol{n} \cdot \boldsymbol{f} \\ f_{\mathrm{t}} = \boldsymbol{t}_{\mathrm{f}} \cdot \boldsymbol{f} = \| \boldsymbol{f}_{\mathrm{t}} \|, \boldsymbol{t}_{\mathrm{f}} \equiv \dfrac{\boldsymbol{f}_{\mathrm{t}}}{\| \boldsymbol{f}_{\mathrm{t}} \|} \ \ (\boldsymbol{n} \cdot \boldsymbol{f}_{\mathrm{t}} = 0, \| \boldsymbol{f}_{\mathrm{f}} \| = 1) \end{cases} \tag{10}$$

The minus sign is added for f_{n} to be positive when the compressive stress acts to the main body by the counter body.

3 Hyperelastic sliding behavior

The hyperelastic-based plastic constitutive relation is adopted in order to formulate the rigorous constitutive equation for sliding phenomenon, while the elastic sliding displacement is quite small because it is induced by the elastic deformation of the surface asperities which are infinitesimally small compared with the contact surface. Then, let the contact stress vector $\boldsymbol{f}$ be given by the hyperelastic relation with the elastic sliding energy function $\varphi(\overline{\boldsymbol{u}}^{\mathrm{e}})$ as

$$\boldsymbol{f} = \frac{\partial \varphi(\overline{\boldsymbol{u}}^{\mathrm{e}})}{\partial \overline{\boldsymbol{u}}^{\mathrm{e}}} \tag{11}$$

Then, the elastic sliding work w^{e} done during the elastic sliding is uniquely determined by the elastic

sliding displacement $\bar{\boldsymbol{u}}^{\mathrm{e}}$ before and after the elastic sliding as Eq. (12):

$$w^{\mathrm{e}}=\int_{\bar{\boldsymbol{u}}_0^{\mathrm{e}}}^{\bar{\boldsymbol{u}}^{\mathrm{e}}}\boldsymbol{f}\cdot\mathrm{d}\bar{\boldsymbol{u}}^{\mathrm{e}}=\int_{\bar{\boldsymbol{u}}_0^{\mathrm{e}}}^{\bar{\boldsymbol{u}}^{\mathrm{e}}}\frac{\partial\varphi(\bar{\boldsymbol{u}}^{\mathrm{e}})}{\partial\bar{\boldsymbol{u}}^{\mathrm{e}}}\cdot\mathrm{d}\bar{\boldsymbol{u}}^{\mathrm{e}}=(\varphi(\bar{\boldsymbol{u}}^{\mathrm{e}}))_{\bar{\boldsymbol{u}}_0^{\mathrm{e}}}^{\bar{\boldsymbol{u}}^{\mathrm{e}}}=\varphi(\bar{\boldsymbol{u}}^{\mathrm{e}})-\varphi(\bar{\boldsymbol{u}}_0^{\mathrm{e}}) \tag{12}$$

Let the following simplest elastic sliding energy function $\varphi(\bar{\boldsymbol{u}}^{\mathrm{e}})$ in the quadratic form be adopted.

$$\varphi(\bar{\boldsymbol{u}}^{\mathrm{e}})=\bar{\boldsymbol{u}}^{\mathrm{e}}\cdot\bar{\boldsymbol{E}}\bar{\boldsymbol{u}}^{\mathrm{e}}/2 \tag{13}$$

where the second-order tensor $\bar{\boldsymbol{E}}$ designates the elastic contact tangent stiffness modulus fulfilling the symmetry $\bar{\boldsymbol{E}}=\bar{\boldsymbol{E}}^{\mathrm{T}}$. The substitution of Eq. (13) into Eq. (11) leads to

$$\boldsymbol{f}=\bar{\boldsymbol{E}}\bar{\boldsymbol{u}}^{\mathrm{e}},\ \bar{\boldsymbol{u}}^{\mathrm{e}}=\bar{\boldsymbol{E}}^{-1}\boldsymbol{f} \tag{14}$$

Assuming the isotropy on the contact surface, i.e. the independence of frictional property to a sliding direction on the contact surface and introducing the normalized rectangular coordinate system $(\bar{\boldsymbol{e}}_1,\bar{\boldsymbol{e}}_2,\bar{\boldsymbol{e}}_3)=(\bar{\boldsymbol{e}}_1,\bar{\boldsymbol{e}}_2,\boldsymbol{n})$ fixed to the contact surface, the elastic contact tangent stiffness modulus tensor $\bar{\boldsymbol{E}}$ is given as Eq. (15):

$$\begin{cases}\bar{\boldsymbol{E}}=\alpha_{\mathrm{t}}(\boldsymbol{I}-\boldsymbol{n}\otimes\boldsymbol{n})+\alpha_{\mathrm{n}}\boldsymbol{n}\otimes\boldsymbol{n}=\alpha_{\mathrm{t}}(\bar{\boldsymbol{e}}_1\otimes\bar{\boldsymbol{e}}_1+\bar{\boldsymbol{e}}_2\otimes\bar{\boldsymbol{e}}_2)+\alpha_{\mathrm{n}}\boldsymbol{n}\otimes\boldsymbol{n}\\ \bar{\boldsymbol{E}}^{-1}=\dfrac{1}{\alpha_{\mathrm{t}}}(\boldsymbol{I}-\boldsymbol{n}\otimes\boldsymbol{n})+\dfrac{1}{\alpha_{\mathrm{t}}}\boldsymbol{n}\otimes\boldsymbol{n}=\dfrac{1}{\alpha_{\mathrm{t}}}(\bar{\boldsymbol{e}}_1\otimes\bar{\boldsymbol{e}}_1+\bar{\boldsymbol{e}}_2\otimes\bar{\boldsymbol{e}}_2)+\dfrac{1}{\alpha_{\mathrm{n}}}\boldsymbol{n}\otimes\boldsymbol{n}\end{cases} \tag{15}$$

where α_{n} and α_{t} are the normal and tangential elastic contact moduli, respectively. Equation (14) with Eq. (15) leads to

$$\boldsymbol{f}=\alpha_{\mathrm{t}}\bar{\boldsymbol{u}}_{\mathrm{t}}^{\mathrm{e}}+\alpha_n\bar{\boldsymbol{u}}_{\mathrm{t}}^{\mathrm{e}},\quad \bar{\boldsymbol{u}}^{\mathrm{e}}=\frac{1}{\alpha_{\mathrm{t}}}\boldsymbol{f}_{\mathrm{t}}+\frac{1}{\alpha_{\mathrm{n}}}\boldsymbol{f}_{\mathrm{n}} \tag{16}$$

4 Elastoplastic sliding velocity

The plastic sliding velocity is formulated based on the subloading surface concept and the tangential-associated flow rule in this section.

4.1 Sliding normal-yield and sliding subloading surfaces

Firstly, let the sliding normal-yield surface and the sliding subloading surface, which passes through the current contact stress and is similar to the sliding normal-yield surface, be given by

$$f(\boldsymbol{f})=\mu \tag{17}$$

$$f(\boldsymbol{f})=r\mu \tag{18}$$

where μ is the sliding hardening/softening function, and r is the sliding normal-yield ratio, i.e., the ratio of the size of the sliding–subloading surface to that of the sliding normal-yield surface as shown in Fig. 1.

Here, Eq. (19) holds for the isotropic yield stress function.

$$\begin{aligned}\frac{\partial f(\boldsymbol{f})}{\partial\boldsymbol{f}}&=\frac{\partial f(f_{\mathrm{t}},f_{\mathrm{n}})}{\partial\boldsymbol{f}}=\frac{\partial f(f_{\mathrm{t}},f_{\mathrm{n}})}{\partial f_{\mathrm{t}}}\frac{\partial f_{\mathrm{t}}}{\partial\boldsymbol{f}}+\frac{\partial f(f_{\mathrm{t}},f_{\mathrm{n}})}{\partial f_{\mathrm{n}}}\frac{\partial f_{\mathrm{n}}}{\partial\boldsymbol{f}}\\&=\frac{\partial f(f_{\mathrm{t}},f_{\mathrm{n}})}{\partial f_{\mathrm{t}}}\boldsymbol{t}_{\mathrm{f}}-\frac{\partial f(f_{\mathrm{t}},f_{\mathrm{n}})}{\partial f_{\mathrm{n}}}\boldsymbol{n}\end{aligned} \tag{19}$$

Then, the consistency condition for the sliding subloading surface in Eq. (18) is given by

$$\frac{\partial f(\boldsymbol{f})}{\partial\boldsymbol{f}}\cdot\dot{\boldsymbol{f}}=r\dot{\mu}+\dot{r}\mu \tag{20}$$

The evolution rule of the sliding hardening/softening function μ is given as Eq. (21) (Fig. 2):

$$\dot{\mu}=-\kappa(\mu-\mu_{\mathrm{k}})\|\dot{\bar{\boldsymbol{u}}}^{\mathrm{p}}\|+\xi(\mu_{\mathrm{s}}-\mu)\quad(\mu_{\mathrm{k}}\le\mu\le\mu_{\mathrm{s}}) \tag{21}$$

i.e.

$$\mathrm{d}\mu=-\kappa(\mu-\mu_{\mathrm{k}})\|\mathrm{d}\bar{\boldsymbol{u}}^{\mathrm{p}}\|+\xi(\mu_{\mathrm{s}}-\mu)\mathrm{d}t\quad(\mu_{\mathrm{k}}\le\mu\le\mu_{\mathrm{s}})$$

where μ_{s} and μ_{k} are the maximum and the minimum values of the sliding hardening/softening function μ, respectively, while let μ_{s} and μ_{k} be called the static

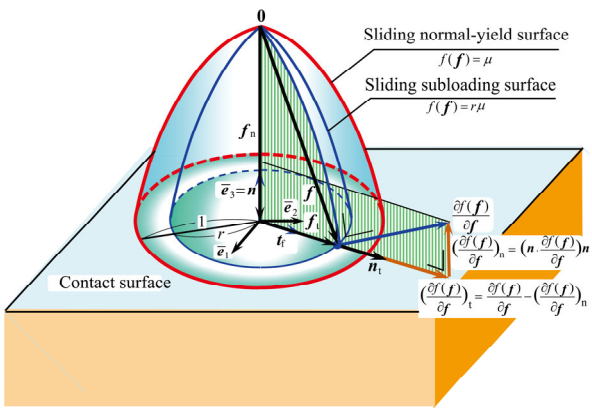

Fig. 1 Sliding normal-yield and subloading surfaces.

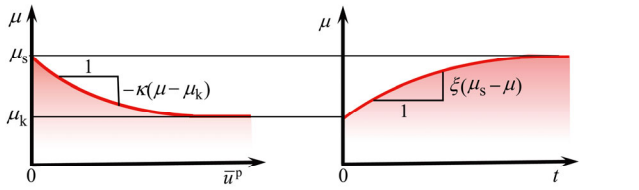

(a) Fast sliding process: $\|\mathrm{d}\bar{\boldsymbol{u}}^{\mathrm{p}}\| \gg \mathrm{d}t$ (b) Quasi-static sliding process: $\|\mathrm{d}\bar{\boldsymbol{u}}^{\mathrm{p}}\| \ll \mathrm{d}t$

Fig. 2 Variation of sliding hardening function. Reproduced with permission from Ref. [32], © Elsevier Ltd. 2004.

and the kinetic sliding hardening function, respectively. κ is the material constant specifying the decrease of the sliding hardening function μ, i.e., $\mathrm{d}\mu$ per a unit plastic displacement $\|\mathrm{d}\bar{\boldsymbol{u}}^{\mathrm{p}}\|$, and ξ is the material constant specifying the increasing (recovering) rate of μ, i.e. $\mathrm{d}\mu$ per a unit time increment $\mathrm{d}t$.

Note: Let the microscopic background of Eq. (21) be given here. The following relation would hold between the sliding hardening function and the ratio of the real contact area to the apparent contact area.

$$\mu = \tau_{\mathrm{m}} r_{\mathrm{a}}, \text{ i.e., } r_{\mathrm{a}} = \mu/\tau_{\mathrm{m}} \tag{22}$$

where τ_{m} is the material constant designating the friction sliding resistance per unit apparent contact area, and r_{a} is the ratio of the real contact area a_{R} to the apparent contact area a_{A}, called the real contact area ratio. i.e.,

$$r_{\mathrm{a}} = \frac{a_{\mathrm{R}}}{a_{\mathrm{A}}} (\le 1) \tag{23}$$

Then, the following relation would hold from the time-derivative of Eq. (22) with Eq. (21).

$$\dot{\mu} = \tau_{\mathrm{m}} \dot{r}_{\mathrm{a}}, \ \dot{r}_{\mathrm{a}} = -\kappa \frac{\mu - \mu_{\mathrm{k}}}{\tau_{\mathrm{m}}} \| \dot{\bar{\boldsymbol{u}}}^{\mathrm{p}} \| + \xi \frac{\mu_{\mathrm{s}} - \mu}{\tau_{\mathrm{m}}} \tag{24}$$

On the other hand, the relation $r_{\mathrm{a}} = 1 - \exp(-bf_{\mathrm{n}})$ (b is the material constant) proposed for rubbers by Ozaki et al. [39] is irrelevant to the plastic sliding history, so that it would not hold in metals.

The rate of the sliding normal-yield ratio r is given by

$$\dot{r} = \bar{U}(r) \| \dot{\bar{\boldsymbol{u}}}^{\mathrm{p}} \| \ (\dot{\bar{\boldsymbol{u}}}^{\mathrm{p}} \neq \boldsymbol{0}) \tag{25}$$

with

$$\bar{U}(r) = \tilde{u} \cot\left(\frac{\pi}{2} r\right) \begin{cases} > 0 & (r < 1) \\ = 0 & (r = 1) \\ < 0 & (r > 1) \end{cases} \tag{26}$$

where $\tilde{u}$ is the material constant (cf. Hashiguchi [12, 13]). The contact stress is automatically attracted to the sliding normal-yield surface in the plastic sliding process, and it is pulled back to that surface even when it goes over the surface in numerical calculation because of $\dot{r} < 0$ for $r > 1$ from Eq. (25) with Eq. (26), as shown in Fig. 3.

4.2 Plastic sliding velocity and elastoplastic sliding velocity

The plastic sliding velocity, the sliding velocity, and the contact stress rate are formulated in the following.

The substitution of Eqs. (21) and (25) into Eq. (20) leads to

$$\frac{\partial f(\boldsymbol{f})}{\partial \boldsymbol{f}} \cdot \dot{\boldsymbol{f}} = r[-\kappa(\mu - \mu_{\mathrm{k}}) \| \dot{\bar{\boldsymbol{u}}}^{\mathrm{p}} \| + \xi(\mu_{\mathrm{s}} - \mu)] + \bar{U}(r) \| \dot{\bar{\boldsymbol{u}}}^{\mathrm{p}} \| \mu \tag{27}$$

Now, assume the tangential-associated flow rule [12]:

$$\dot{\bar{\boldsymbol{u}}}^{\mathrm{p}} = \dot{\bar{\lambda}} \boldsymbol{n}_{\mathrm{t}} \ (\dot{\bar{\lambda}} \ge 0)(\| \dot{\bar{\boldsymbol{u}}}^{\mathrm{p}} \| = \dot{\bar{\lambda}}, \boldsymbol{n} \cdot \dot{\bar{\boldsymbol{u}}}^{\mathrm{p}} = 0) \tag{28}$$

where

$$\boldsymbol{n}_{\mathrm{t}} \equiv \left(\frac{\partial f(\boldsymbol{f})}{\partial \boldsymbol{f}} \right)_{\mathrm{t}} \Bigg/ \left\| \left(\frac{\partial f(\boldsymbol{f})}{\partial \boldsymbol{f}} \right)_{\mathrm{t}} \right\| \ (\| \boldsymbol{n}_{\mathrm{t}} \| = 1, \ \boldsymbol{n} \cdot \boldsymbol{n}_{\mathrm{t}} = 0) \tag{29}$$

with

$$\left(\frac{\partial f(\boldsymbol{f})}{\partial \boldsymbol{f}} \right)_{\mathrm{t}} \equiv \frac{\partial f(\boldsymbol{f})}{\partial \boldsymbol{f}} - \left(\boldsymbol{n} \cdot \frac{\partial f(\boldsymbol{f})}{\partial \boldsymbol{f}} \right) \boldsymbol{n} = (\boldsymbol{I} - \boldsymbol{n} \otimes \boldsymbol{n}) \frac{\partial f(\boldsymbol{f})}{\partial \boldsymbol{f}} \tag{30}$$

where $\dot{\bar{\lambda}}$ and $\boldsymbol{n}_{\mathrm{t}}$ are the magnitude and the direction, respectively, of the plastic sliding velocity.

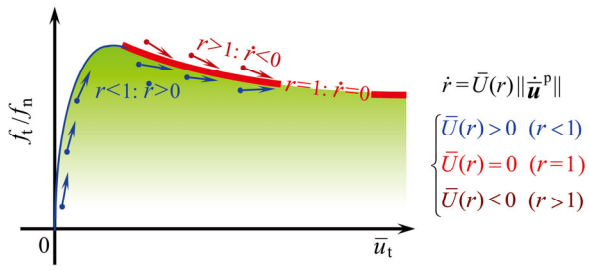

Fig. 3 Contact stress controlling function in subloading-friction model: Contact stress is automatically attracted to sliding normal-yield surface in plastic sliding process. Reproduced with permission from Ref. [32], © Elsevier Ltd. 2004.

The substitution of Eq. (28) into Eq. (27) leads to

$$\frac{\partial f(\boldsymbol{f})}{\partial \boldsymbol{f}}\cdot\dot{\boldsymbol{f}}=\dot{\bar{\lambda}}m^{\mathrm{p}}+m^{\mathrm{c}} \tag{31}$$

where

$$m^{\mathrm{p}}\equiv-\kappa(\mu-\mu_{\mathrm{k}})r+\bar{U}(r)\mu,\ \ m^{\mathrm{c}}\equiv\xi(\mu_{\mathrm{s}}-\mu)r\ \ (\geq 0) \tag{32}$$

The positive plastic multiplier $\dot{\bar{\lambda}}$ is derived from Eq. (31) as Eq. (33):

$$\dot{\bar{\lambda}}=\frac{\dfrac{\partial f(\boldsymbol{f})}{\partial \boldsymbol{f}}\cdot\dot{\boldsymbol{f}}-m^{\mathrm{c}}}{m^{\mathrm{p}}},\ \ \dot{\bar{\boldsymbol{u}}}^{\mathrm{p}}=\frac{\dfrac{\partial f(\boldsymbol{f})}{\partial \boldsymbol{f}}\cdot\dot{\boldsymbol{f}}-m^{\mathrm{c}}}{m^{\mathrm{p}}}\boldsymbol{n}_{\mathrm{t}} \tag{33}$$

Then, the rate of sliding displacement is given by substituting Eqs. (14) and (33) into Eq. (4) as Eq. (34):

$$\dot{\bar{\boldsymbol{u}}}=\bar{\boldsymbol{E}}^{-1}\dot{\boldsymbol{f}}+\frac{\dfrac{\partial f(\boldsymbol{f})}{\partial \boldsymbol{f}}\cdot\dot{\boldsymbol{f}}-m^{\mathrm{c}}}{m^{\mathrm{p}}}\boldsymbol{n}_{\mathrm{t}} \tag{34}$$

It follows from Eq. (34) that

$$\frac{\partial f(\boldsymbol{f})}{\partial \boldsymbol{f}}\cdot\bar{\boldsymbol{E}}\dot{\bar{\boldsymbol{u}}}=\frac{\partial f(\boldsymbol{f})}{\partial \boldsymbol{f}}\cdot\dot{\boldsymbol{f}}+\frac{\dfrac{\partial f(\boldsymbol{f})}{\partial \boldsymbol{f}}\cdot\dot{\boldsymbol{f}}-m^{\mathrm{c}}}{m^{\mathrm{p}}}\frac{\partial f(\boldsymbol{f})}{\partial \boldsymbol{f}}\cdot\bar{\boldsymbol{E}}\boldsymbol{n}_{\mathrm{t}}$$

leading to

$$\frac{\partial f(\boldsymbol{f})}{\partial \boldsymbol{f}}\cdot\bar{\boldsymbol{E}}\dot{\bar{\boldsymbol{u}}}=m^{\mathrm{p}}\frac{\dfrac{\partial f(\boldsymbol{f})}{\partial \boldsymbol{f}}\cdot\dot{\boldsymbol{f}}-m^{\mathrm{c}}}{m^{\mathrm{p}}}-m^{\mathrm{c}}+\frac{\dfrac{\partial f(\boldsymbol{f})}{\partial \boldsymbol{f}}\cdot\dot{\boldsymbol{f}}-m^{\mathrm{c}}}{m^{\mathrm{p}}}\frac{\partial f(\boldsymbol{f})}{\partial \boldsymbol{f}}\cdot\bar{\boldsymbol{E}}\boldsymbol{n}_{t}$$

i.e.,

$$\frac{\partial f(\boldsymbol{f})}{\partial \boldsymbol{f}}\cdot\bar{\boldsymbol{E}}\dot{\bar{\boldsymbol{u}}}\left(=m^{\mathrm{p}}\dot{\bar{\lambda}}-m^{\mathrm{c}}+\dot{\bar{\lambda}}\frac{\partial f(\boldsymbol{f})}{\partial \boldsymbol{f}}\cdot\bar{\boldsymbol{E}}\boldsymbol{n}_{\mathrm{t}}\right)=\left(m^{\mathrm{p}}+\frac{\partial f(\boldsymbol{f})}{\partial \boldsymbol{f}}\cdot\bar{\boldsymbol{E}}\boldsymbol{n}_{\mathrm{t}}\right)\dot{\bar{\lambda}}-m^{\mathrm{c}}$$

from which the plastic multiplier in terms of the sliding velocity, denoted by the symbol $\dot{\bar{\Lambda}}$, is given by Eq. (35):

$$\dot{\bar{\Lambda}}=\frac{\dfrac{\partial f(\boldsymbol{f})}{\partial \boldsymbol{f}}\cdot\bar{\boldsymbol{E}}\dot{\bar{\boldsymbol{u}}}-m^{\mathrm{c}}}{m^{\mathrm{p}}+\dfrac{\partial f(\boldsymbol{f})}{\partial \boldsymbol{f}}\cdot\bar{\boldsymbol{E}}\boldsymbol{n}_{\mathrm{t}}},\ \ \dot{\bar{\boldsymbol{u}}}^{\mathrm{p}}=\frac{\dfrac{\partial f(\mathbf{f})}{\partial \mathbf{f}}\cdot\bar{\boldsymbol{E}}\dot{\bar{\boldsymbol{u}}}-m^{\mathrm{c}}}{m^{\mathrm{p}}+\dfrac{\partial f(\boldsymbol{f})}{\partial \boldsymbol{f}}\cdot\bar{\boldsymbol{E}}\boldsymbol{n}_{\mathrm{t}}} \tag{35}$$

Then, the inverse relation of Eq. (34) is given by Eq. (36):

$$\dot{\boldsymbol{f}}=\bar{\boldsymbol{E}}(\dot{\bar{\boldsymbol{u}}}-\dot{\bar{\Lambda}}\boldsymbol{n}_{\mathrm{t}})=\left(\bar{\boldsymbol{E}}-\frac{\bar{\boldsymbol{E}}\boldsymbol{n}_{\mathrm{t}}\otimes\dfrac{\partial f(\boldsymbol{f})}{\partial \boldsymbol{f}}\bar{\boldsymbol{E}}}{m^{\mathrm{p}}+\dfrac{\partial f(\boldsymbol{f})}{\partial \boldsymbol{f}}\cdot\bar{\boldsymbol{E}}\boldsymbol{n}_{\mathrm{t}}}\right)\dot{\bar{\boldsymbol{u}}}+\frac{m^{\mathrm{c}}}{m^{\mathrm{p}}+\dfrac{\partial f(\boldsymbol{f})}{\partial \boldsymbol{f}}\cdot\bar{\boldsymbol{E}}\boldsymbol{n}_{\mathrm{t}}}\bar{\boldsymbol{E}}\boldsymbol{n}_{\mathrm{t}} \tag{36}$$

The loading criterion is given as Eq. (37) [12]:

$$\begin{cases}\dot{\bar{\boldsymbol{u}}}^{\mathrm{p}}\neq\boldsymbol{0} & \text{for}\ \ \dot{\bar{\Lambda}}>0\ \ \text{or}\ \ \dfrac{\partial f(\boldsymbol{f})}{\partial \boldsymbol{f}}\cdot\bar{\boldsymbol{E}}\dot{\bar{\boldsymbol{u}}}-m^{\mathrm{c}}>0\\ \dot{\bar{\boldsymbol{u}}}^{\mathrm{p}}=\boldsymbol{0} & \text{for others}\end{cases} \tag{37}$$

5 Sliding-yield surface with saturation of tangential contact stress

Now, we adopt the following sliding-yield stress function $f(\boldsymbol{f})=f(f_{\mathrm{t}},f_{\mathrm{n}})$ in Eq. (17):

$$f(\boldsymbol{f})=f(f_{\mathrm{t}},f_{\mathrm{n}})=\frac{f_{\mathrm{t}}}{g_{\mathrm{n}}(f_{\mathrm{n}})} \tag{38}$$

leading to the sliding normal-yield surface (Fig. 4):

$$f_{\mathrm{t}}/g_{\mathrm{n}}=\mu,\ \ \text{i.e.,}\ f_{\mathrm{t}}=g_{\mathrm{n}}\mu \tag{39}$$

where $g_{\mathrm{n}}=g_{\mathrm{n}}(f_{\mathrm{n}})\ (<1)$ is the function of f_{n}, satisfying the conditions:

$$g_{\mathrm{n}}=\begin{cases}=0 & \text{for}\ \ f_{\mathrm{n}}=0\\ \to 1\ \ (f_{\mathrm{t}}=\mu) & \text{for}\ \ f_{\mathrm{n}}\to\infty\end{cases} \tag{40}$$

$$g_{\mathrm{n}}'\equiv\frac{dg_{\mathrm{n}}}{df_{\mathrm{n}}}=\begin{cases}c_{\mathrm{n}} & \text{for}\ \ f_{\mathrm{n}}=0\\ \to 0 & \text{for}\ \ f_{\mathrm{n}}\to\infty\end{cases} \tag{41}$$

leading to

$$\frac{\partial f_{\mathrm{t}}}{\partial f_{\mathrm{n}}}=g_{\mathrm{n}}'\mu=\begin{cases}c_{\mathrm{n}}\mu & \text{for}\ \ f_{\mathrm{n}}=0\\ \to 0 & \text{for}\ \ f_{\mathrm{n}}\to\infty\end{cases} \tag{42}$$

where c_{n} is the material constant with the inverse dimension of stress. Equation (39) represents the sliding normal-yield surface with the fusiform shape, which expands from the origin to the positive direction of the normal contact stress f_{n} in the three-dimensional stress space $(f_{\mathrm{t1}},f_{\mathrm{t2}},f_{\mathrm{n}})$. The tangential contact stress

f_t on the sliding normal-yield surface increases with the normal contact stress f_n and saturates at $f_t = \mu$, while it approaches faster to the saturation (maximum) value μ for a larger value of c_n, as shown in Fig. 4(a). The sliding normal-yield and the sliding subloading surfaces satisfying Eqs. (40) and (41) are shown in Fig. 4(b).

The following differentiations hold for Eq. (38).

$$\frac{\partial f(\boldsymbol{f})}{\partial f_t} = \frac{1}{g_n}, \quad \frac{\partial f(\boldsymbol{f})}{\partial f_n} = -\frac{f_t}{g_n^2} g_n' \tag{43}$$

$$\frac{\partial f(\boldsymbol{f})}{\partial \boldsymbol{f}} = \frac{1}{g_n^2}(g_n \boldsymbol{t}_f + f_t g_n' \boldsymbol{n}) \tag{44}$$

noting Eq. (19). Further, it follows from Eqs. (19) and (29) that

$$\boldsymbol{n}_t = \boldsymbol{t}_f \left(\left(\frac{\partial f(\boldsymbol{f})}{\partial \boldsymbol{f}} \right)_t = \frac{\partial f(f_t, f_n)}{\partial f_t} \boldsymbol{t}_f \right) \tag{45}$$

$$\bar{\boldsymbol{E}} \boldsymbol{n}_t = \bar{\boldsymbol{E}} \boldsymbol{t}_f = \alpha_t \boldsymbol{t}_f \tag{46}$$

$$\begin{aligned} \bar{\boldsymbol{E}} \frac{\partial f(\boldsymbol{f})}{\partial \boldsymbol{f}} &= [\alpha_t (\boldsymbol{I} - \boldsymbol{n} \otimes \boldsymbol{n}) + \alpha_n \boldsymbol{n} \otimes \boldsymbol{n}] \frac{1}{g_n^2}(g_n \boldsymbol{t}_f + f_t g_n' \boldsymbol{n}) \\ &= \frac{1}{g_n^2}(\alpha_t g_n \boldsymbol{t}_f + \alpha_n f_f g_n' \boldsymbol{n}) \end{aligned} \tag{47}$$

$$\frac{\partial f(\boldsymbol{f})}{\partial \boldsymbol{f}} \cdot \bar{\boldsymbol{E}} \boldsymbol{t}_f = \frac{1}{g_n^2}(\alpha_t g_n \boldsymbol{t}_f + \alpha_n f_t g_n' \boldsymbol{n}) \cdot \alpha_t \boldsymbol{t}_f = \frac{\alpha_t}{g_n} \tag{48}$$

$$\frac{\partial f(\boldsymbol{f})}{\partial \boldsymbol{f}} \cdot \bar{\boldsymbol{E}} \dot{\bar{\boldsymbol{u}}} = \frac{1}{g_n^2}(\alpha_t g_n \boldsymbol{t}_f + \alpha_n f_t g_n' \boldsymbol{n}) \cdot \dot{\bar{\boldsymbol{u}}} \tag{49}$$

The substitutions of Eqs. (44)–(49) into Eqs. (34)–(36) lead to

$$\begin{aligned} \dot{\bar{\boldsymbol{u}}} = &\left[\frac{1}{\alpha_t}(\boldsymbol{I} - \boldsymbol{n} \otimes \boldsymbol{n}) + \frac{1}{\alpha_n} \boldsymbol{n} \otimes \boldsymbol{n} \right] \dot{\boldsymbol{f}} \\ &+ \frac{\frac{1}{g_n^2}(\alpha_t g_n \boldsymbol{t}_f + \alpha_n f_t g_n' \boldsymbol{n}) \cdot \dot{\boldsymbol{f}} - m^c}{m^p} \boldsymbol{n}_t \end{aligned} \tag{50}$$

$$\begin{aligned} \dot{\boldsymbol{f}} = &[\alpha_t (\boldsymbol{I} - \boldsymbol{n} \otimes \boldsymbol{n}) + \alpha_n \boldsymbol{n} \otimes \boldsymbol{n}] \\ &\left[\dot{\bar{\boldsymbol{u}}} - \alpha_t \left\langle \frac{\frac{1}{g_n^2}(\alpha_t g_n \boldsymbol{t}_f + \alpha_n f_t g_n' \boldsymbol{n}) \cdot \dot{\bar{\boldsymbol{u}}} - m^c}{m^p + \alpha_t / g_n} \right\rangle \boldsymbol{t}_f \right] \end{aligned} \tag{51}$$

or

$$\dot{\boldsymbol{f}} = \bar{\boldsymbol{E}}^{ep} \dot{\bar{\boldsymbol{u}}} + \alpha_t \frac{m^c}{m^p + \alpha_t / g_n} \boldsymbol{t}_f \tag{52}$$

with

$$\begin{aligned} \bar{\boldsymbol{E}}^{ep} \equiv &\alpha_t (\boldsymbol{I} - \boldsymbol{n} \otimes \boldsymbol{n}) + \alpha_n \boldsymbol{n} \otimes \boldsymbol{n} \\ &- \frac{\alpha_t \boldsymbol{t}_f \otimes \frac{1}{g_n^2}(\alpha_t g_n \boldsymbol{t}_f + \alpha_n f_t g_n' \boldsymbol{n})}{m^p + \alpha_t / g_n} \end{aligned} \tag{53}$$

Let the explicit function satisfying Eqs. (40) and (41) be given by Eq. (54):

$$g_n = 1 - \exp(-c_n f_n), \quad g_n' = c_n \exp(-c_n f_n) \tag{54}$$

Eqations (44)–(51) with Eq. (54) are expressed in the coordinate system $(\bar{\boldsymbol{e}}_1, \bar{\boldsymbol{e}}_2, \boldsymbol{n})$ as Eqs. (55)–(59):

$$\frac{\partial f(\boldsymbol{f})}{\partial \boldsymbol{f}} = \frac{1}{g_n^2}[g_n (t_{f1} \bar{\boldsymbol{e}}_1 + t_{f2} \bar{\boldsymbol{e}}_2) + c_n f_t \exp(-c_n f_n) \boldsymbol{n}] \tag{55}$$

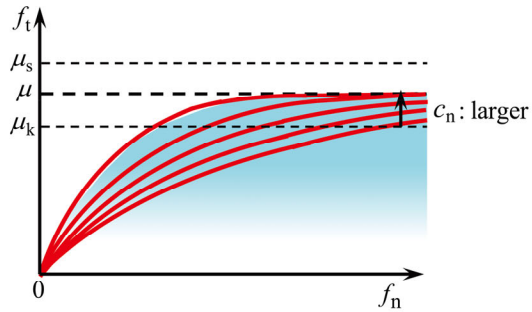

(a) Sliding normal-yield surface $f(\boldsymbol{f})(= f_t / g_n) = \mu$, which is fatter for larger material constant c_n.

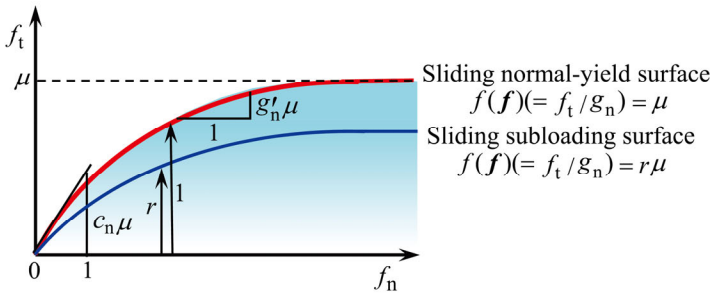

(b) Sliding normal-yield and subloading surfaces.

Fig. 4 Sliding normal-yield and subloading surfaces with saturation of tangential contact stress.

$$\bar{\boldsymbol{E}}\frac{\partial f(\boldsymbol{f})}{\partial \boldsymbol{f}}=\frac{1}{g_{\mathrm{n}}^{2}}[\alpha_{\mathrm{t}}g_{\mathrm{n}}(\boldsymbol{t}_{\mathrm{f1}}\bar{\boldsymbol{e}}_{1}+\boldsymbol{t}_{\mathrm{f2}}\bar{\boldsymbol{e}}_{2})+\alpha_{\mathrm{n}}c_{\mathrm{n}}f_{\mathrm{t}}\exp(-c_{\mathrm{n}}f_{\mathrm{n}})\boldsymbol{n}] \tag{56}$$

$$\bar{\boldsymbol{E}}\dot{\bar{\boldsymbol{u}}}=[\alpha_{\mathrm{t}}(\bar{\boldsymbol{e}}_{1}\otimes\bar{\boldsymbol{e}}_{1}+\bar{\boldsymbol{e}}_{2}\otimes\bar{\boldsymbol{e}}_{2})+\alpha_{\mathrm{n}}\boldsymbol{n}\otimes\boldsymbol{n}]\dot{\bar{\boldsymbol{u}}} \tag{57}$$

$$\frac{\partial f(\boldsymbol{f})}{\partial \boldsymbol{f}}\cdot\bar{\boldsymbol{E}}\dot{\bar{\boldsymbol{u}}}=\frac{1}{g_{\mathrm{n}}^{2}}[\alpha_{\mathrm{t}}g_{\mathrm{n}}(\boldsymbol{t}_{\mathrm{f1}}\bar{\boldsymbol{e}}_{1}+\boldsymbol{t}_{\mathrm{f2}}\bar{\boldsymbol{e}}_{2})+\alpha_{\mathrm{n}}c_{\mathrm{n}}f_{\mathrm{t}}\exp(-c_{\mathrm{n}}f_{\mathrm{n}})\boldsymbol{n}]\cdot\dot{\bar{\boldsymbol{u}}} \tag{58}$$

The following eight material constants are involved in the present friction model, and they are determined as follows.

α_{n} and α_{t} may be given large values for metals because they are microscopically based on the elastic deformation of the surface asperities. Here, note that they are necessary in order to formulate as the elastoplasticity by avoiding the rigid-plasticity in which the stress increment cannot be determined uniquely for the input of sliding displacement increment.

μ_{s} and μ_{k} are determined, such that the tangential contact stress coincides with the peak and the bottom values, respectively, in the linear sliding process under the infinitely large constant normal contact stress.

κ and ξ are determined to describe the decrease and the recovery, respectively, of the sliding hardening function μ.

$\tilde{u}$ is determined to describe the increasing rate of the contact stress for the plastic sliding rate.

c_{n} is determined to designate the dependence of the ratio of the tangential vs. normal contact stress on the normal contact stress.

6 Numerical experiments

The principal mechanical responses of the present subloading-friction model will be examined by performing the numerical experiments in this section. The material parameters are chosen with the two levels of the static sliding hardening functions μ_{s} as:

$$\alpha_{\mathrm{n}}=5{,}000\ \mathrm{MPa}\cdot\mathrm{mm}^{-3},\quad \alpha_{\mathrm{t}}=5{,}000\ \mathrm{MPa}\cdot\mathrm{mm}^{-3};$$
$$\mu_{\mathrm{s}}=10{,}000\ \text{and}\ 7{,}500\ \mathrm{MPa},\quad \mu_{\mathrm{k}}=7{,}000\ \mathrm{MPa};$$
$$\kappa=15{,}000\ \mathrm{mm}^{-1},\quad \xi=110\ \mathrm{s}^{-1},\quad \tilde{u}=15\ \mathrm{mm}^{-1},$$
$$c_{\mathrm{n}}=0.0002\ \mathrm{MPa}^{-1}$$

and the tangential sliding velocity is chosen as $\dot{\bar{\boldsymbol{u}}}_{\mathrm{t}}$ = 1 mm·min^{-1}.

Firstly, the tangential contact stress paths at five levels of constant normal contact stress are shown in Fig. 5,

$$\begin{aligned}\dot{\boldsymbol{f}}&=[\alpha_{\mathrm{t}}(\bar{\boldsymbol{e}}_{1}\otimes\bar{\boldsymbol{e}}_{1}+\bar{\boldsymbol{e}}_{2}\otimes\bar{\boldsymbol{e}}_{2})+\alpha_{\mathrm{n}}\boldsymbol{n}\otimes\boldsymbol{n}]\left[\dot{\bar{\boldsymbol{u}}}-\alpha_{\mathrm{t}}\left\langle\frac{\frac{1}{g_{\mathrm{n}}^{2}}[\alpha_{\mathrm{t}}(t_{\mathrm{f1}}\bar{\boldsymbol{e}}_{1}+t_{\mathrm{f2}}\bar{\boldsymbol{e}}_{2})+\alpha_{\mathrm{n}}c_{\mathrm{n}}(f_{\mathrm{t}}/g_{\mathrm{n}})\exp(-c_{\mathrm{n}}f_{\mathrm{n}})\boldsymbol{n}]\dot{\bar{\boldsymbol{u}}}-m^{\mathrm{c}}}{m^{\mathrm{p}}+\alpha_{\mathrm{t}}/g_{\mathrm{n}}}\right\rangle(t_{\mathrm{f1}}\bar{\boldsymbol{e}}_{1}+t_{\mathrm{f2}}\bar{\boldsymbol{e}}_{2})\right]\\&=[\alpha_{\mathrm{t}}(\bar{\boldsymbol{e}}_{1}\otimes\bar{\boldsymbol{e}}_{1}+\bar{\boldsymbol{e}}_{2}\otimes\bar{\boldsymbol{e}}_{2})+\alpha_{\mathrm{n}}\boldsymbol{n}\otimes\boldsymbol{n}]\dot{\bar{\boldsymbol{u}}}-\alpha_{\mathrm{t}}(t_{\mathrm{f1}}\bar{\boldsymbol{e}}_{1}+t_{\mathrm{f2}}\bar{\boldsymbol{e}}_{2})\left\langle\frac{\frac{1}{g_{\mathrm{n}}^{2}}[\alpha_{\mathrm{t}}(t_{\mathrm{f1}}\bar{\boldsymbol{e}}_{1}+t_{\mathrm{f2}}\bar{\boldsymbol{e}}_{2})+\alpha_{\mathrm{n}}c_{\mathrm{n}}(f_{\mathrm{t}}/g_{\mathrm{n}})\exp(-c_{\mathrm{n}}f_{\mathrm{n}})\boldsymbol{n}]\dot{\bar{\boldsymbol{u}}}-m^{\mathrm{c}}}{m^{\mathrm{p}}+\alpha_{\mathrm{t}}/g_{\mathrm{n}}}\right\rangle\end{aligned} \tag{59}$$

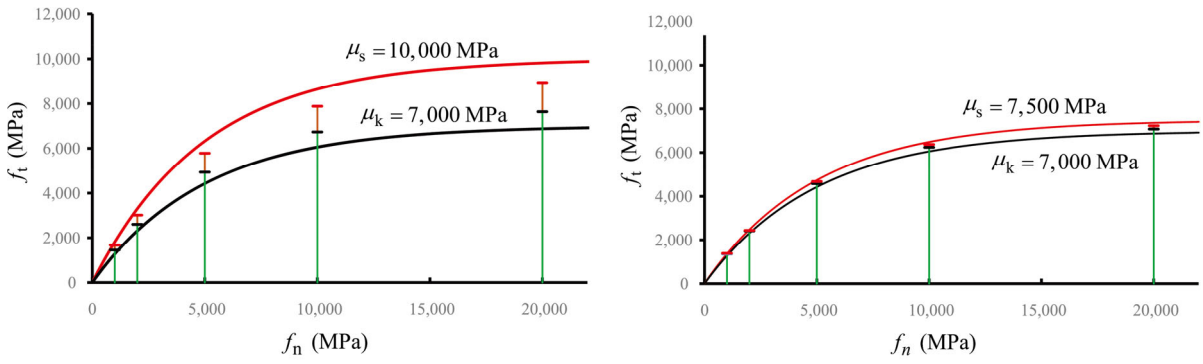

(a) $\mu_{\mathrm{s}}=10{,}000$ MPa and $\mu_{\mathrm{k}}=7{,}000$ MPa (b) $\mu_{\mathrm{s}}=7{,}500$ MPa and $\mu_{\mathrm{k}}=7{,}000$ MPa

Fig. 5 Tangential contact stress paths at five levels of normal contact stress for different static sliding hardening functions. Red short bar in each stress path indicates the maximum contact tangential stress, and black one indicates the contact tangential stress at infinite sliding displacement.

in which the sliding normal-yield surface for the static and the kinetic isotropic hardening functions are depicted by red and black curves, respectively. The maximum contact tangential stress is larger for the larger static sliding hardening function.

Next, the variations of tangential contact stress at the five levels of normal contact stress in the monotonic sliding followed by the reverse sliding for the different static sliding hardening functions are shown in Fig. 6.

The variations of tangential contact stress with the five levels of stationary sliding time just after the unloading for the different static sliding hardening functions in the monotonic and the reciprocal sliding are shown in Figs. 7 and 8, respectively. More remarkable recoveries of the tangential contact stress by the longer stationary sliding time are shown in these figures.

The variations of the tangential contact stress in the pulsating sliding with three levels of stationary sliding time just after the unloading to the zero tangential contact stress is shown in Fig. 9. The recovery of the tangential contact stress with the increase of sliding time is shown, while it decreases gradually with the increase of number of cycles.

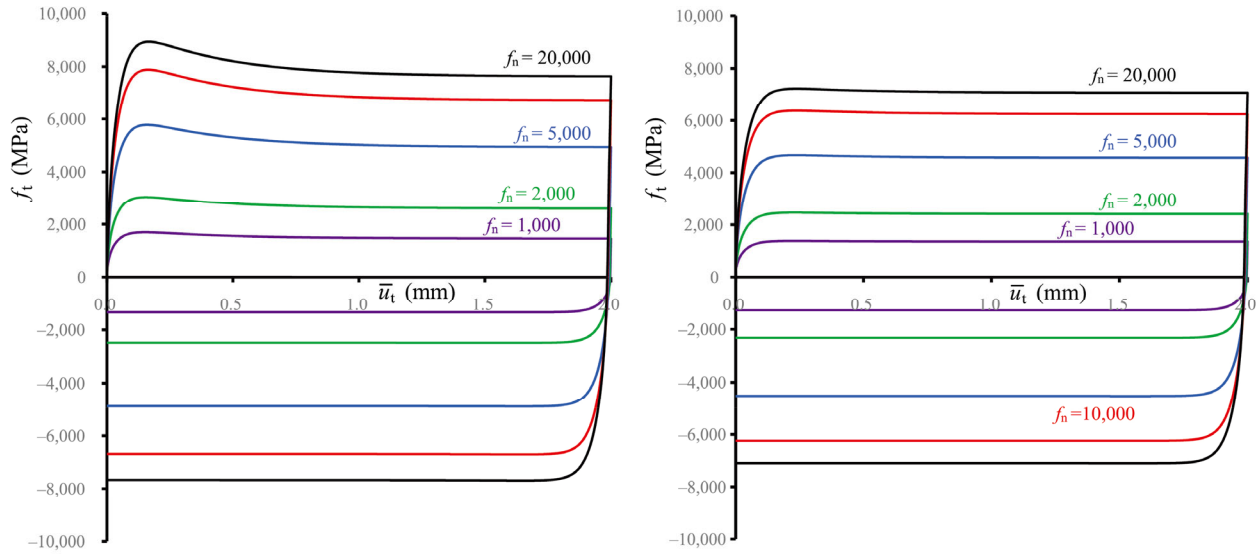

(a) μ_s = 10,000 MPa and μ_k = 7,000 MPa (b) μ_s = 7,500 MPa and μ_k = 7,000 MPa

Fig. 6 Variations of tangential contact stress at five levels of normal contact stress in monotonic sliding, followed by the reverse sliding for different static sliding hardening functions.

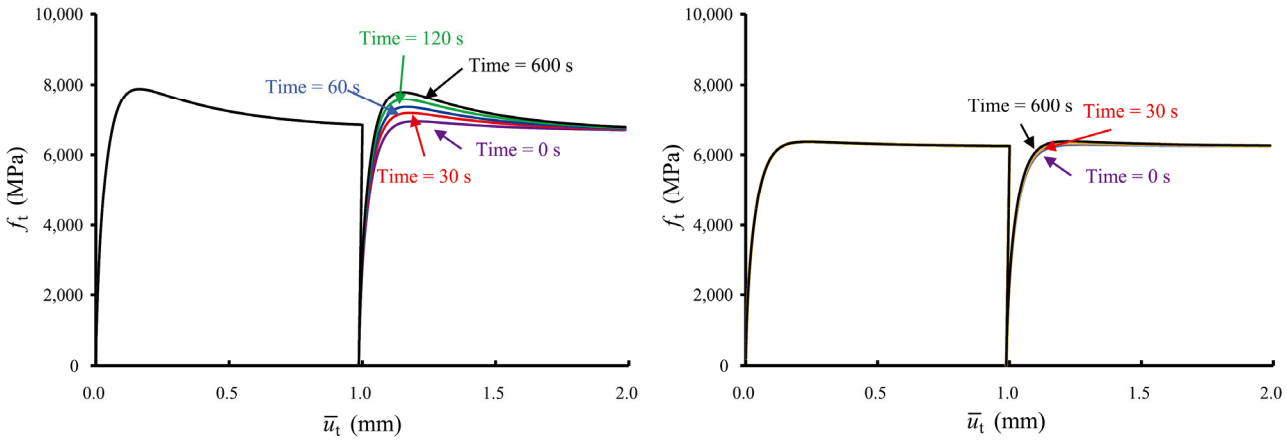

(a) μ_s = 10,000 MPa and μ_k = 7,000 MPa (b) μ_s = 7,500 MPa and μ_k = 7,000 MPa

Fig. 7 Variations of tangential contact stress with five levels of stationary sliding time just after unloading for different static sliding hardening functions.

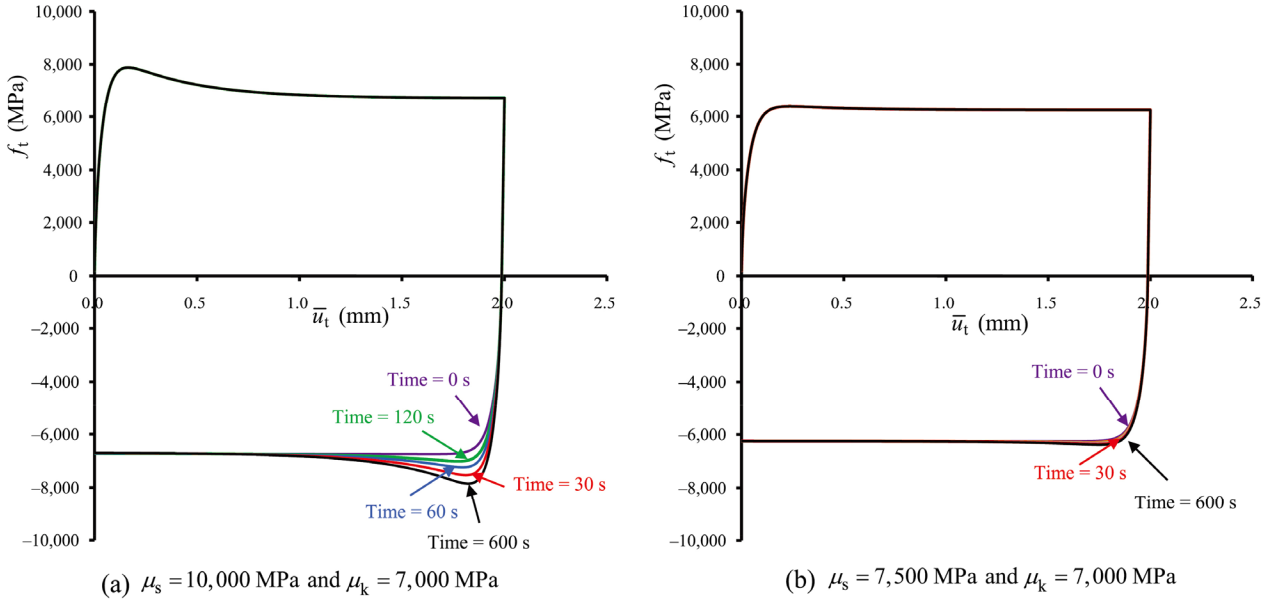

Fig. 8 Variations of tangential contact stress during reciprocal sliding with five levels of stationary sliding time just after unloading for different static sliding hardening functions.

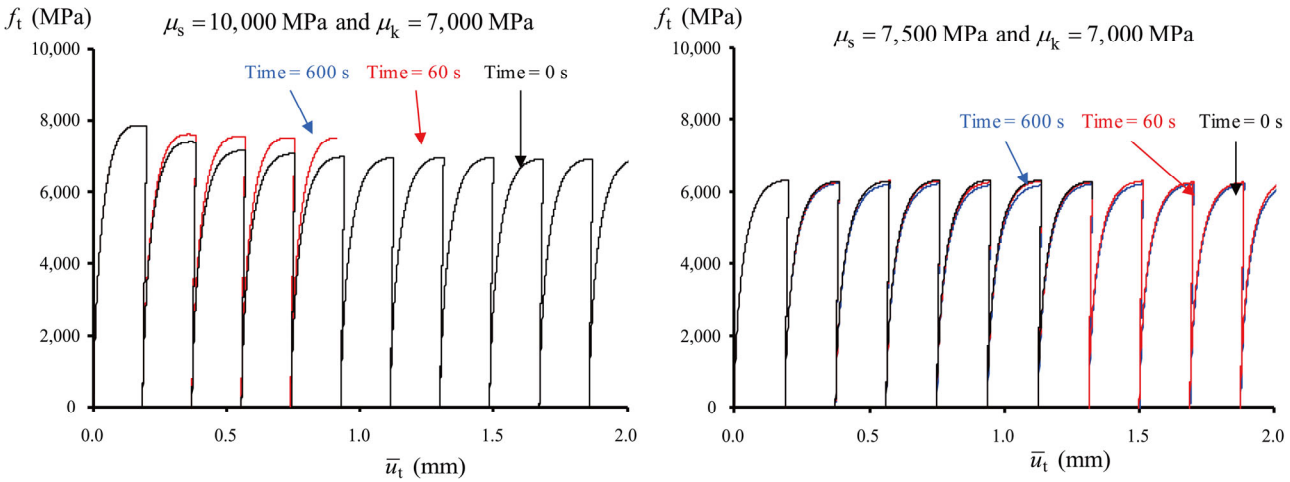

Fig. 9 Variations of tangential contact stress in pulsating contact tangential stress with three levels of stationary sliding time just after unloading for different static sliding hardening functions.

7 Comparison with experiments

The simulation of the test data for the linear sliding behavior for the boric acid lubricated A16111-T4 and tool steel interface in Ref. [14] is shown in Fig. 10 to verify the applicability of the present model to the description of real friction phenomenon. The linear sliding behavior at the constant normal contact stress is the most basic behavior among various sliding behaviors, but strangely, the available test data is quite little as the authors could find only the test data from Ref. [14]. Fortunately, this test data is suitable for the verification of the present model, since the rather high normal contact stress up to 600 MPa is applied in this data. The relations of the contact tangential stress vs. the sliding displacement for the five levels of the constant normal contact stresses are represented, where the values of the material parameters are chosen as

$$\alpha_n = 500\ \text{MPa}\cdot\text{mm}^{-3},\ \alpha_t = 500\ \text{MPa}\cdot\text{mm}^{-3};$$
$$\mu_s = 500\ \text{MPa},\ \mu_k = 63\ \text{MPa};$$
$$\kappa = 98\ \text{mm}^{-1},\ \xi = 11\ \text{s}^{-1},\ \tilde{u} = 15\ \text{mm}^{-1},$$
$$c_n = 0.0002\ \text{MPa}^{-1}$$

while the tangential sliding velocity $\dot{\bar{u}}_t$ is 1 mm·s^{-1} in the test data.

The variations of the tangential contact stress are closely simulated by the present friction model, as shown in Fig. 10.

The comparison for the relations of the tangential contact stress vs. the normal contact stress for four levels of the sliding displacement is shown in Fig. 11, which is depicted from the test and the calculated values. The fact that the ratio of the tangential contact stress to the normal contact stress is not constant but decreases gradually with the increase of the normal contact stress is simulated closely. The incorporation of the present model is required to describe the friction behavior in the test data accurately. A test datum specifying an explicit sliding displacement less than 1 mm is not shown in the figure of Ref. [14]. Then, only the calculated result for the displacement 0.5 mm is shown by the dashed curve in Fig. 11.

The quite close simulation of the test result [14] is attained by the present model. Then, the applicability of the present friction model for the prediction of real friction behavior between metals would be verified. Besides, the simulation of the test data was also performed by Gearing et al. [14]. However, their friction model [11] used for the simulation is

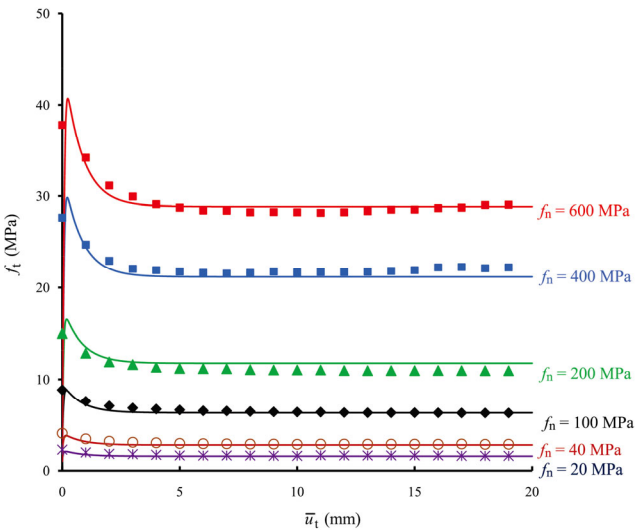

Fig. 10 Comparison of the simulation results and test data of boric acid lubricated A16111-T4/tool steel interface in Ref. [14] for tangential contact stress vs. sliding displacement relations at six levels of normal contact stress, where the calculated results are shown by solid lines.

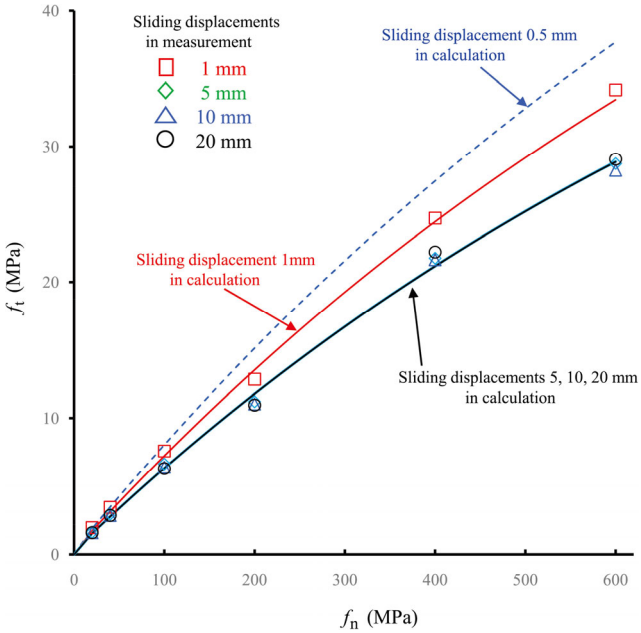

Fig. 11 Comparison of the simulation results and test data of boric acid lubricated A16111-T4/tool steel interface in Ref. [14] for tangential contact stress vs. normal contact stress relations in four levels of sliding displacement, where the calculated results are shown by solid lines. The dashed curve shows the calculated result for the sliding displacement = 0.5 mm.

physically impertinent belonging to the creep model, which is approximately applicable to the sliding behavior at high rate but inapplicable to the sliding behavior at the moderate rate including the quasi-static sliding behavior as delineated in Hashiguchi [12, 13], while the sliding velocity in the test data in Ref. [14] is rather high as $\dot{\bar{u}}_t$ = 1 mm·s^{-1}. On the other hand, the subloading-friction model is concerned with the sliding behavior in the general sliding velocity.

The tangential contact stress lowers to a constant value after it exhibits the peak value, as shown in Figs. 6–8, and 10. Therefore, it would be independent of the sliding displacement for the sliding displacement larger than 5 mm, as shown in Fig. 11. The inconsistent tendency in the test results for the sliding displacement = 5, 10, and 20 mm in this figure would show the difficulty of the precise measurement of the tangential contact stress for a large sliding displacement in tests under a constant normal contact stress.

8 Concluding remarks

The subloading-friction model (Hashiguchi et al.

[32, 33], etc.) is extended in this article. The extended model is summarized to be capable of describing the following principal properties.

1) The smooth transition from the elastic to the plastic transition leads to the continuous variation of the elastoplastic stiffness modulus, which is of the importance for the numerical calculation since the loading criterion, i.e., the judgment whether the plastic sliding induced is not required.

2) The contact stress is automatically pulled back to the normal sliding-yield surface when it goes out from that surface, leading to the highly efficient numerical calculation.

3) The friction decreases from the static to the kinetic friction.

4) The friction resistance recovers during the stationary state of sliding.

5) The tangential contact stress saturates with the increase of the normal contact, so that the tangential contact stress does not exceed the shear strength of the contacting solids.

Property 5 was not furnished in the past subloading-friction model. These principal mechanical characteristics of the proposed model is represented by the numerical experiments for the linear monotonic and the reciprocal sliding with the cease of sliding in the unloaded state. Further, the validity of the present model is verified by the simulation of the test data [14] for metals. The present model will contribute to the development of the boundary value problems for the deformation/sliding of solids and structures subjected to a high normal contact stress.

References

[1] Seguchi Y, Shindo A, Tomita Y, Sunohara M. Sliding rule of friction in plastic forming of metal. *Compt Meth Nonlinear Mech*, University of Texas at Austin, 683–692 (1974)

[2] Fredriksson B. Finite element solution of surface nonlinearities in structural mechanics with special emphasis to contact and fracture mechanics problems. *Comput Struct* **6**(4–5): 281–290 (1976)

[3] Michalowski R, Mróz Z. Associated and non-associated sliding rules in contact friction problems. *Archiv Mech* **30**(3): 259–276 (1978)

[4] Oden J T, Pires E B. Algorithms and numerical results for finite element approximations of contact problems with non-classical friction laws. *Comput Struct* **19**(1–2): 137–147 (1984)

[5] Oden J T, Pires E B. Nonlocal and nonlinear friction laws and variational principles for contact problems in elasticity. *J Appl Mech* **50**(1): 67–76 (1983)

[6] Curnier A. A theory of friction. *Int J Solids Struct* **20**(7): 637–647 (1984)

[7] Cheng J H, Kikuchi N. An incremental constitutive relation of unilateral contact friction for large deformation analysis. *J Appl Mech* **52**(3): 639–648 (1985)

[8] Kikuchi N, Oden J T. *Contact Problems in Elasticity: Society for Industrial and Applied Mathematics*. Philadelphia (USA): Society for Industrial and Applied Mathematics, 1987.

[9] Wriggers P, Vu Van T, Stein E. Finite element formulation of large deformation impact–contact problems with friction. *Comput Struct* **37**(3): 319–331 (1990)

[10] Perić D, Owen D R J. Computational model for 3-D contact problems with friction based on the penalty method. *Int J Numer Methods Eng* **35**(6): 1289–1309 (1992)

[11] Anand L. A constitutive model for interface friction. *Comput Mech* **12**(4): 197–213 (1993)

[12] Hashiguchi K. *Foundations of Elastoplasticity: Subloading Surface Model*, 3rd edn. Springer, 2017.

[13] Hashiguchi, K. *Nonlinear Continuum Mechanics for Finite Elasticity–plasticity: Multiplicative Decomposition with Subloading Surface Model*. Elsevier, 2020.

[14] Gearing B P, Moon H S, Anand L. A plasticity model for interface friction: Application to sheet metal forming. *Int J Plast* **17**(2): 237–271 (2001)

[15] Dieterich J H. Time-dependent friction and the mechanics of stick–slip. *Pure Appl Geophys* **116**(4–5): 790–806 (1978)

[16] Ruina A L. Friction laws and instabilities: A quasistatic analysis of some dry frictional behavior. Ph.D. Thesis. Providence (USA): Brown University, 1980.

[17] Ruina A L. Slip instability and state variable friction laws. *J Geophys Res Solid Earth* **88**(B12): 10359–10370 (1983)

[18] Rice J R, Ruina A L. Stability of steady frictional slipping. *J Appl Mech* **50**(2): 343–349 (1983)

[19] Scholz C H. Rate-and state-variable friction law. *Nature* **391**: 37–41 (1998)

[20] Rice J R, Lapusta N, Ranjith K. Rate and state dependent friction and the stability of sliding between elastically deformable solids. *J Mech Phys Solids* **49**(9): 1865–1898 (2001)

[21] Kame N, Fujita S, Nakatani M, Kusakabe T. Effects of a revised rate- and state-dependent friction law on aftershock triggering model. *Tectonophysics* **600**: 187–195 (2013)

[22] Rabinowicz E. The nature of the static and kinetic coefficients of friction. *J Appl Phys* **22**(11): 1373–1379 (1951)

[23] Howe P G, Benton D P, Puddington I E. London–van der Waals attractive forces between glass surfaces. *Can J Chem* **33**(9): 1375–1383 (1955)

[24] Brockley C A, Davis H R. The time-dependence of static friction. *J Lubr Technol* **90**(1): 35–41 (1968)

[25] Kato S, Sato N, Matsubayashi T. Some considerations on characteristics of static friction of machine tool slideway. *J Lubr Technol* **94**(3): 234–247 (1972)

[26] Horowitz F G, Ruina A L. Slip patterns in a spatially homogeneous fault model. *J Geophys Res* **94**(B8): 10279–10298 (1989)

[27] Bureau L, Baumberger T, Caroli C, Ronsin O. Low-velocity friction between macroscopic solids. *Comptes Rendus De l'académie Des Sci Ser IV Phys* **2**(5): 699–707 (2001)

[28] Oldroyd J G. On the formulation of rheological equations of state. *Proc Roy Soc A Mat Phys Eng Sci* **200**(1063): 523–541 (1950)

[29] Hashiguchi K, Yamakawa Y. *Introduction to Finite Strain Theory for Continuum Elasto-plasticity*. Chichester (UK): John Wiley & Sons, 2012.

[30] Wriggers P. *Computational Contact Mechanics*. Berlin (Germany): Springer Berlin Heidelberg, 2006.

[31] Popov V L. *Contact Mechanics and Friction: Physical Principles and Applications*. Berlin (Germany): Springer Berlin Heidelberg, 2017.

[32] Hashiguchi K, Ozaki S, Okayasu T. Unconventional friction theory based on the subloading surface concept. *Int J Solids Struct* **42**(5–6): 1705–1727 (2005)

[33] Hashiguchi K, Ozaki S. Constitutive equation for friction with transition from static to kinetic friction and recovery of static friction. *Int J Plast* **24**(11): 2102–2124 (2008)

[34] Ozaki T, Yamakawa Y, Ueno M, Hashiguchi K. Description of sand–metal friction behavior based on subloading-friction model. *Friction* **10**: 1660–1675 (2022)

[35] Ozaki S, Hashiguchi K. Numerical analysis of stick–slip instability by a rate-dependent elastoplastic formulation for friction. *Tribol Int* **43**(11): 2120–2133 (2010)

[36] Hashiguchi K. *Elastoplasticity Theory*. Berlin (Germany): Springer Berlin Heidelberg, 2009.

[37] Ozaki S, Hikida K, Hashiguchi K. Elastoplastic formulation for friction with orthotropic anisotropy and rotational hardening. *Int J Solids Struct* **49**(3–4): 648–657 (2012)

[38] Hashiguchi K, Ueno M, Kuwayama T, Suzuki N, Yonemura S, Yoshikawa N. Constitutive equation of friction based on the subloading-surface concept. *Proc Roy Soc A Mat Phys Eng Sci* **472**(2191): 20160212 (2016)

[39] Ozaki S, Matsuura T, Maegawa S. Rate-, state-, and pressure-dependent friction model based on the elastoplastic theory. *Friction* **8**(4): 768–783 (2020)

[40] Hashiguchi K. Multiplicative hyperelastic-based plasticity for finite elastoplastic deformation/sliding: A comprehensive review. *Arch Comput Methods Eng* **26**(3): 597–637 (2019)

Koichi HASHIGUCHI. He received his Ph.D. degree from Tokyo Institute of Technology, Japan, in 1976. After that he served as assistant professor, associate professor, and professor at Kyushu University, Japan. He is currently an emeritus professor at Kyushu University, member of the Engineering Academy of Japan, and the technical adviser of MSC software Ltd., Japan. His research area covers the elasto-plastic deformation and the friction phenomena of solids, proposing the subloading surface model.

Masami UENO. He received his Ph.D. degree of agriculture from the University of Tsukuba, Japan, in 1983. He has worked in the Department of Agricultural Engineering, University of the Ryukyus, Japan. He is currently an emeritus professor at the University. His research covers the solid mechanics, smart farming, and systems engineering for agriculture.